

Calculation of elastic constants of embedded-atom-model potentials in the NVT ensemble

Menahem Krief* and Yinon Ashkenazy

Racah Institute of Physics, The Hebrew University, 9190401 Jerusalem, Israel

A method for the calculation of elastic constants in the NVT ensemble, using molecular dynamics (MD) simulation with a realistic many-body embedded-atom-model (EAM) potential, is studied in detail. It is shown that in such NVT MD simulations, the evaluation of elastic constants is robust and accurate, as it gives the elastic tensor in a single simulation which converges using a small number of time steps and particles. These results highlight the applicability of this method in: (i) the calculation of local elastic constants of non-homogeneous crystalline materials and (ii) in the calibration of interatomic potentials, as a fast and accurate alternative to the common method of explicit deformation, which requires a set of consistent simulations at different conditions. The method is demonstrated for the calculation of the elastic constants of copper in the temperature range of 0-1000K, and results agree with the target values used for the potential calibration. The various contributions to the values of the elastic constants, namely, the Born, stress fluctuation and ideal gas terms, are studied as a function of temperature.

I. INTRODUCTION

The calculation of thermo-elastic properties of materials using computer simulations, plays a key role in understanding the response of materials to deformation under varying conditions. In a wide range of applications, material structure leads to local variation in the elastic response functions, due to grain boundaries and hetero-phase interfaces. It is this local variation of elastic properties that allow tailoring of the macroscopic effective material properties. The development of a model for the relation between composite material specific local property and an effective average response function depends on understanding how local properties contribute and interact in order to generate an observable average response. Furthermore, local elastic properties are not accessible experimentally for a wide range of systems, and so reliable numerical evaluation of these may play a key role in the development of effective models for composite materials.

While it is well established that various thermal and mechanical properties can be evaluated for various atomistic structures by atomistic simulations, it is also well established that such evaluation requires addressing non pairwise terms. The widely used embedded atom model (EAM)[1], is a fast, simple and accurate method, which allows a correct description of the microscopic interactions in crystalline materials. Molecular dynamics calculations of adiabatic elastic constants (which are performed in the microcanonical NVE ensemble), for metallic elements, using EAM model potentials, were performed in the past [2–4], based on the widely used formulation of Ray et al. [5].

In this manuscript we present and analyze the feasibility, robustness and accuracy of the calculation of elastic

constants of metals under constant temperature and volume, that is, in the canonical NVT ensemble. Using the stress-stress formulation [4, 6–9], all the components of the elastic constant tensor are obtained in a single molecular dynamics simulation, as opposed to the common explicit deformation method [8, 10–16], which requires several simulations under different deformations. In addition, the method allows the evaluation of elastic properties in localized regions within larger non-homogeneous simulation box, unlike first principle methods which allow efficient temperature dependent calculations, but only for a uniform system [17, 18]. Finally, it is demonstrated that NVT calculations of elastic constants converge more rapidly in comparison to the NPT strain-strain fluctuations formulation [8, 9, 19–21], using symplectic numerical integrators [22–27] and Nose-Hoover thermostat chain [28–30].

We performed calculations of the isothermal elastic constants C_{11}, C_{12}, C_{44} of Copper for a widely used realistic tabulated EAM potential by Mishin et al. [31]. This potential successfully reproduces energy and stability of several nonequilibrium configurations as well as transformation paths between different structures. The calculations were compared with experimental results in the temperature range 0-1000K, and a good agreement is achieved. The manuscript is structured as follows: We start with a short review of formalism used from thermoelasticity, then we describe in detail how elastic constants can be calculated using a single MD simulation in the NVT ensemble in Section 3, and conclude with Section 4 in which we employ the described method to calculate elastic constants in Copper for a commonly used EAM potential.

II. THERMOELASTICITY

We start with a brief review of the definitions and notations of thermo-elasticity, that will be used throughout

* menahem.krief@mail.huji.ac.il

the manuscript. Given a deformation from a reference configuration \mathbf{R} to a configuration $\mathbf{r} = \mathbf{r}(\mathbf{R})$, the Lagrangian strain tensor is defined by:

$$\eta_{\alpha\beta} = \frac{1}{2} \left(\frac{\partial r_\gamma}{\partial R_\alpha} \frac{\partial r_\gamma}{\partial R_\beta} - \delta_{\alpha\beta} \right), \quad (1)$$

where Greek indices such as α, β, γ represent Cartesian components, for which we employ Einstein summation convention. In matrix notation, the strain tensor is related to the Jacobian (metric) tensor:

$$J_{\alpha\beta} = \frac{\partial r_\alpha}{\partial R_\beta}, \quad (2)$$

by:

$$\boldsymbol{\eta} = \frac{1}{2} (\mathbf{J}^T \mathbf{J} - \mathbf{I}), \quad (3)$$

where \mathbf{I} is the identity matrix. The difference in dimensions due to deformation can thus be written using the strain tensor 1 via:

$$\delta r^2 - \delta R^2 = 2\eta_{\alpha\beta} \delta R_\alpha \delta R_\beta. \quad (4)$$

And the mechanical work due to an infinitesimal deformation with Lagrangian strain $d\eta_{\alpha\beta}$ is given by [32–37]:

$$\delta W/V_0 = -\tau_{\alpha\beta} d\eta_{\alpha\beta}, \quad (5)$$

where V_0 is the undeformed volume and the thermodynamic tension tensor, also known as the second Piola-Kirchhoff stress tensor [32], is defined by:

$$\boldsymbol{\tau} = \det(\mathbf{J}) \mathbf{J}^{-1} \boldsymbol{\sigma} \mathbf{J}^{-T}, \quad (6)$$

where $\boldsymbol{\sigma}$ is the Cauchy stress tensor, and the ‘ $-T$ ’ superscript denotes matrix transposition and inversion. We note that $\boldsymbol{\tau} = \boldsymbol{\sigma}$ for a zero applied strain ($\mathbf{J} = \mathbf{I}$, $\boldsymbol{\eta} = \mathbf{0}$). If the deformation process is reversible (an assumption which excludes plasticity), then the first law of thermodynamics for the internal energy \mathcal{E} is written as:

$$d\mathcal{E} = Td\mathcal{S} + V_0 \tau_{\alpha\beta} d\eta_{\alpha\beta}, \quad (7)$$

where T denotes the temperature and \mathcal{S} the entropy. And changes in the free energy

$$d\mathcal{F} = \mathcal{S}dT + V_0 \tau_{\alpha\beta} d\eta_{\alpha\beta}. \quad (8)$$

The thermodynamic tension tensor is the thermodynamic conjugate of the Lagrangian strain tensor:

$$\tau_{\alpha\beta} = \frac{1}{V_0} D_{\alpha\beta} \mathcal{F}, \quad (9)$$

where we used the symmetrical partial derivative operator:

$$D_{\alpha\beta} = \frac{1}{2} \left(\frac{\partial}{\partial \eta_{\alpha\beta}} + \frac{\partial}{\partial \eta_{\beta\alpha}} \right), \quad (10)$$

due to symmetry of the strain tensor $d\eta_{\alpha\beta} = d\eta_{\beta\alpha}$ in eq. 8. The Taylor expansion of the elastic free energy around the un-deformed state, $\boldsymbol{\eta} = \mathbf{0}$, is written as:

$$\mathcal{F}(\boldsymbol{\eta})/V_0 = \mathcal{F}(\mathbf{0})/V_0 + \sigma_{\alpha\beta} \eta_{\alpha\beta} + \frac{1}{2} C_{\alpha\beta\gamma\delta} \eta_{\alpha\beta} \eta_{\gamma\delta} + \dots \quad (11)$$

where:

$$\sigma_{\alpha\beta} = \tau_{\alpha\beta}(\boldsymbol{\eta} = \mathbf{0}) = \frac{1}{V_0} D_{\alpha\beta} \mathcal{F} \Big|_{\boldsymbol{\eta}=\mathbf{0}}, \quad (12)$$

and the second order isothermal elastic constants are defined by:

$$C_{\alpha\beta\gamma\delta} = \frac{1}{V_0} D_{\alpha\beta} D_{\gamma\delta} \mathcal{F} \Big|_{\boldsymbol{\eta}=\mathbf{0}}, \quad (13)$$

where the derivatives in equations 12-13 are taken at constant T and evaluated at zero strain $\boldsymbol{\eta} = \mathbf{0}$.

III. MOLECULAR DYNAMICS AND ELASTIC CONSTANTS

In this section we briefly outline how the entire isothermal elasticity tensor can be obtained in a single molecular dynamics simulation using the stress-stress fluctuation method [2, 5, 8, 9, 36, 38]. This method is favorable over the widely used explicit deformation method [8, 11–16], which requires multiple simulations under various deformations, in order to obtain different components of the elasticity tensor.

Starting from the Hamiltonian of a system of N particles is written as:

$$\mathcal{H}(\mathbf{r}^N, \mathbf{p}^N) = \sum_i \frac{p_i^2}{2m_i} + \mathcal{V}(\mathbf{r}_1, \dots, \mathbf{r}_N), \quad (14)$$

where m_i, \mathbf{r}^N and \mathbf{p}^N denotes, respectively, the masses, position and momentum vectors of the N particles. The embedded-atom-model (EAM) potential [1], is defined by a pair potential $v = v(r)$, an embedding function $F = F(\rho)$ and a local electron density function $\rho = \rho(r)$, so that the the potential energy takes the form:

$$\mathcal{V}(\mathbf{r}_1, \dots, \mathbf{r}_N) = \sum_i F(\rho_i) + \sum_{i < j} v(r_{ij}), \quad (15)$$

where $\mathbf{r}_{ij} = \mathbf{r}_i - \mathbf{r}_j$ is the interatomic displacement vector and the electron density function of particle i is given by $\rho_i = \sum_{j \neq i} \rho(r_{ij})$. For an EAM potential of the form 15, the force on a particle i can be written as:

$$\mathbf{F}_i = \sum_{j \neq i} F_{ij} \frac{\mathbf{r}_{ij}}{r_{ij}}, \quad (16)$$

where:

$$F_{ij} = -(v'(r_{ij}) + [F'(\rho_i) + F'(\rho_j)]\rho'(r_{ij})). \quad (17)$$

The instantaneous kinetic temperature is given by:

$$\frac{1}{2}k_B T_K = \frac{1}{g} \sum_i \frac{p_i^2}{2m_i}, \quad (18)$$

where k_B is Boltzmann's constant and $g = 3(N - 1)$ is the number of degrees of freedom. The instantaneous pressure tensor $P_{\alpha\beta}$ is obtained from the virial theorem:

$$P_{\alpha\beta}V = \sum_i \left(\frac{p_{i,\alpha}p_{i,\beta}}{m_i} + r_{i,\alpha}F_{i,\beta} \right).$$

Where V is the system volume. The total pressure is given by the average of the diagonal components:

$$P = \frac{1}{3}(P_{11} + P_{22} + P_{33}). \quad (19)$$

For an EAM potential, it follows from eq. 16 that:

$$\sum_i r_{i,\alpha}F_{i,\beta} = \sum_{i<j} F_{ij} \frac{r_{ij,\alpha}r_{ij,\beta}}{r_{ij}}$$

so that the pressure tensor has the form:

$$P_{\alpha\beta}V = \sum_i \frac{p_{i,\alpha}p_{i,\beta}}{m_i} + \sum_{i<j} F_{ij} \frac{r_{ij,\alpha}r_{ij,\beta}}{r_{ij}} \quad (20)$$

It can be shown [3, 6–9, 39, 40], as detailed in Appendix A, that in the NVT ensemble, the elastic constants 13 are given by:

$$C_{\alpha\beta\gamma\delta} = \langle C_{\alpha\beta\gamma\delta}^B \rangle - \frac{V}{k_B T} [\langle \sigma_{\alpha\beta}^B \sigma_{\gamma\delta}^B \rangle - \langle \sigma_{\alpha\beta}^B \rangle \langle \sigma_{\gamma\delta}^B \rangle] + \frac{Nk_B T}{V} (\delta_{\alpha\gamma}\delta_{\beta\delta} + \delta_{\alpha\delta}\delta_{\beta\gamma}), \quad (21)$$

where $\langle \cdot \rangle$ represents ensemble average. The last term in eq. 21 is a non configurational ideal gas contribution which vanishes at zero temperature and is related to volume derivatives with respect to the strain tensor. The first term in eq. 21, known as the Born term, is a configurational part which is given by a canonical average of the zero-temperature expression for the elastic constant [5, 8, 41]. The second term in eq. 21 accounts for stress fluctuations and also vanishes at zero temperature (this term is obtained directly from the general identity A11 detailed in Appendix A). The Born stress tensor in eq. 21 is defined by the derivative of the potential energy with respect to strain, evaluated at a state of zero applied strain:

$$\sigma_{\alpha\beta}^B = \frac{1}{V} D_{\alpha\beta} \mathcal{V} \Big|_{\eta=0}. \quad (22)$$

The Cauchy stress tensor is given by:

$$\sigma_{\alpha\beta} = \langle \sigma_{\alpha\beta}^B \rangle - \frac{k_B T N}{V} \delta_{\alpha\beta} \quad (23)$$

Similarly, the Born elastic constant term is given by:

$$C_{\alpha\beta\gamma\delta}^B = \frac{1}{V} D_{\alpha\beta} D_{\gamma\delta} \mathcal{V} \Big|_{\eta=0}. \quad (24)$$

For an EAM potential of the form 15, it can be shown that the Born stress has the following form:

$$V\sigma_{\alpha\beta}^B = - \sum_{i<j} F_{ij} \frac{r_{ij,\alpha}r_{ij,\beta}}{r_{ij}}, \quad (25)$$

while the Born elastic constant takes the form [2–4, 7]:

$$VC_{\alpha\beta\gamma\delta}^B = \sum_{i<j} X_{ij} \frac{r_{ij,\alpha}r_{ij,\beta}r_{ij,\gamma}r_{ij,\delta}}{r_{ij}^2} + \sum_i F''(\rho_i) g_{i,\alpha\beta} g_{i,\gamma\delta}, \quad (26)$$

where:

$$X_{ij} = v''(r_{ij}) - \frac{1}{r_{ij}} v'(r_{ij}) + (F'(\rho_i) + F'(\rho_j)) \left(\rho''(r_{ij}) - \frac{1}{r_{ij}} \rho'(r_{ij}) \right), \quad (27)$$

and:

$$g_{i,\alpha\beta} = \sum_{k \neq i} \rho'(r_{ik}) \frac{r_{ik,\alpha}r_{ik,\beta}}{r_{ik}}. \quad (28)$$

For completeness, a detailed derivation of equations 21–28, is given in Appendix A.

IV. RESULTS

Detailed molecular dynamics simulations are performed, in order to demonstrate and analyze the formalism developed in the previous sections, which we employ for the calculation of the elasticity tensor of copper.

The results presented in this work were obtained using a newly developed molecular dynamics code. The computational model employs symplectic numerical integrators, which preserve phase space measures of non-Hamiltonian dynamics [22–27], incorporates Nose-Hoover thermostat chains in the NVT and NPT ensembles [28–30], solved using high order Suzuki-Yoshida decomposition [44, 45]. The equations of motions are detailed in appendices B and C, for the NVT and NPT ensembles, respectively.

The isothermal elastic constants of Copper were calculated as a function of temperature using a series of molecular dynamics calculations in the NVT ensemble employing a widely used EAM potential by Mishin et al. [31].

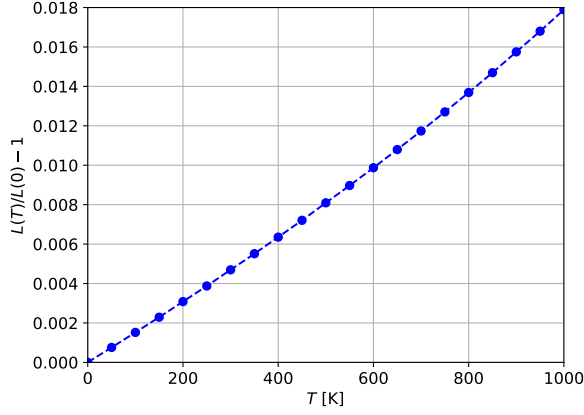


Figure 1. The thermal expansion ratio $L(T)/L(0) - 1$ of Copper, as a function of temperature, resulting from a series of NPT molecular dynamics simulations at zero pressure in the temperature range 0-1000K. Time dependent measures of the simulation at $T=300\text{K}$ are presented in detail in figures 2-3.

This potential is calibrated so that the calculated zero temperature fcc lattice constant is $L(T=0) = 3.615\text{\AA}$ and the elastic constants are given by $C_{11} = 169.9\text{GPa}$, $C_{12} = 122.6\text{GPa}$ and $C_{44} = 76.2\text{GPa}$ (the Voigt notation will be used throughout this section). In the simulations presented below, a cubical system with 500 atoms was used with their initial positions on an fcc lattice, and initial velocities sampled from a Maxwell distribution at the appropriate temperature. Periodic boundary conditions were used. The integration of the equations of motion was performed with a time step of 2fs for 2×10^5 steps. A Nose-Hoover thermostat chain of size $M = 10$ and a relaxation time of $\tau_T = 50\text{fs}$ was applied.

The NVT calculations require prior evaluation of the equilibrium volume at zero stress at the various temperatures. These volumes can be evaluated using known thermal expansion coefficient, but we re-evaluated them using a series of zero stress NPT calculations. These yield the lattice constant as a function of temperature, $L(T)$. The resulting equilibrium thermal expansion ratio, $L(T)/L(0) - 1$, is shown as a function of temperature in Fig. 1. An analysis of the thermalization and convergence of a selected NPT simulation at $T = 300\text{K}$ is presented in detail in figures 2-3. It is evident that convergence is achieved relatively fast with $N = 10^4$ MD steps. The instantaneous pressure tensor is shown in Fig. 3, demonstrating that the pressure is equilibrated to zero. The NPT simulations were initialized with an fcc lattice with the zero temperature lattice constant $L(T=0) = 3.615\text{\AA}$, which is then subsequently relaxed to the equilibrium value $L(T)$ at zero pressure (as seen in Fig. 2). A barostat, coupled to a Nose-Hoover thermostat chain of size $M' = 10$ with a relaxation time of $\tau_P = 500\text{fs}$ was used.

Results of a specific NVT simulation with $T = 300\text{K}$ and a volume chosen such that the total pressure is zero,

are shown in figures 4-5. Fig. 4 shows the components of the Born stress tensor (defined in eq. 25) throughout the simulation. As expected, only the diagonal ideal gas terms are nonzero (since the total pressure is zero, from eq. 23 we have $\langle \sigma_{\alpha\beta}^B \rangle = \delta_{\alpha\beta} k_B T N/V$). Fig. 5 shows the Born elastic constants $C_{11}^B, C_{12}^B, C_{44}^B$ given in eq. 26, as in Fig. 2. It is evident that the Born elastic constants are converged relatively fast, at about 10^4 MD steps.

In Fig. 6 we show the conservation of the energy like quantities for both the NPT (given in eq. C15) and NVT calculations and NVT (given in eq. B8) throughout the simulations discussed above. It is evident that a good conservation of about 10^{-5} is maintained throughout the simulation, which highlights the great advantages of measure preserving integrators of the non-Hamiltonian dynamical systems [23, 24].

In Fig. 7 the isothermal elastic constants as a function of temperature are plotted, together with the contributions of the Born term, the Born stress fluctuation term and the ideal gas kinetic term (see eq. 21). As expected, it is evident that the reduction of the elastic constant with increasing temperature is mainly due to the stress fluctuations term, which is larger at higher temperatures. It is also evident that in the temperature range studied here, the ideal gas contribution is negligible.

Finally, in Fig. 8, we compare the calculated isothermal elastic constants as a function of temperature, with experimental results. In Ref. [42], experimental results for isothermal elastic constants C_{11}, C_{12}, C_{44} are given in the temperature range 0-300K. In Ref. [43], experimental results for adiabatic elastic constants are given in the range 300-800K. Since the isothermal and adiabatic elastic constants are identical for C_{44} , we can use these experimental results directly. On the other hand, the isothermal and adiabatic elastic constants C_{11}, C_{12} are not identical [46-48][46-48], and were not compared here. It is evident that the agreement between the calculated and experimental values is relatively good, especially given the fact that the Copper potential we used [31] was calibrated to slightly different values at $T = 0\text{K}$ (the experimental values of Ref. [42] are $C_{11} = 176.2\text{GPa}$, $C_{12} = 124.94\text{GPa}$ and $C_{44} = 81.77\text{GPa}$). The values that were used to calibrate the tabulated potential (at $T = 0$), are reproduced by our calculations to 5 significant digits. In addition, in Ref. [10] adiabatic elastic constants are calculated by molecular dynamics simulations (using LAMMPS MD code [49]) at $T = 300\text{K}$, using the same EAM potential and employing the explicit deformation method. This result for C_{44} is also shown in Fig. 8, showing a very good agreement with our calculation (less than 0.5%).

and at results calculated with the same potential (and using LAMMPS [49]), The blue X data point represents the computational C_{44} result given in Ref. [10]

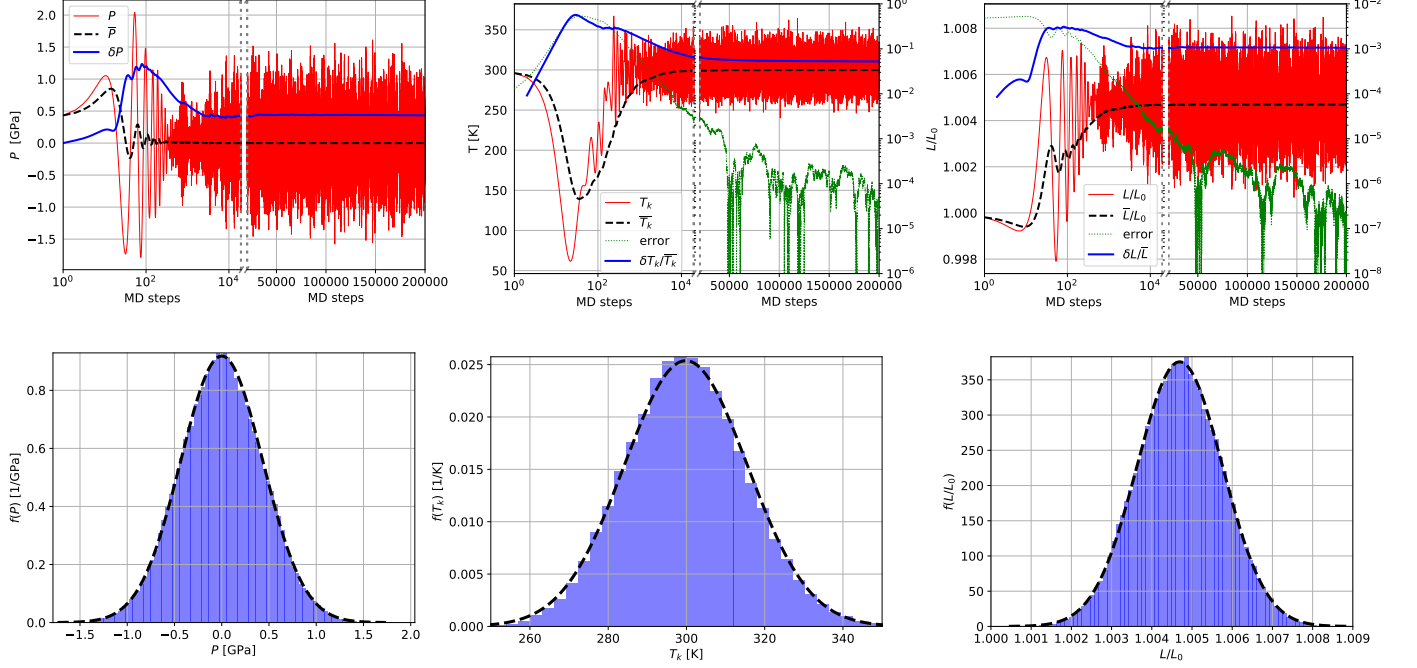


Figure 2. (Color online) Analysis of a molecular dynamics simulation of Copper in the NPT ensemble at zero pressure and $T = 300\text{K}$. The upper left figure shows the instantaneous pressure (eq. 19, red solid line), the cumulative average pressure (black dashed line) and the cumulative pressure standard deviation. The upper middle figure shows the instantaneous kinetic temperature (eq. 18, red solid line, left y-axis), the cumulative average temperature (black dashed line, left y-axis), the relative error between the current cumulative average value to the the final average value (green dotted line) and the ratio between the cumulative standard deviation to the cumulative average (blue solid line, right axis). Similarly, the upper right figure shows the results for the ratio between the simulation box length and the initial box length ($L_0 = 3.165\text{\AA}$). The first 2×10^4 steps are plotted on a logarithmic x scale, in order to show the initial thermalization period. The lower figures show histograms and fitted Gaussian distributions for the values of the instantaneous pressure (lower left), temperature (middle figure) and box size ratio (lower right).

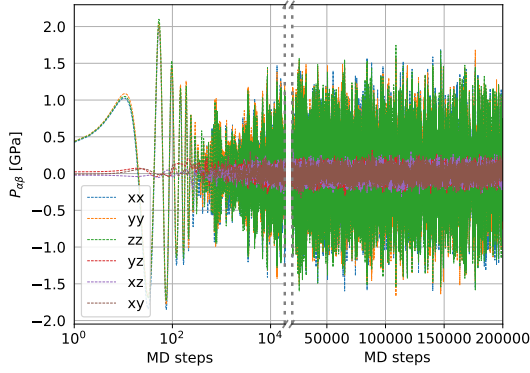


Figure 3. (Color online) Components of the instantaneous pressure tensor (eq. 18) for the NPT simulation described in Fig. 2.

V. SUMMARY

The elasticity tensor of copper, modeled with a realistic tabulated EAM potential, was calculated using a single molecular dynamics simulation in the NVT ensemble, employing the stress-stress fluctuation formulation. It was shown that such calculations are accurate and robust and converge within a few thousand MD steps, with a relatively small number of particles (a few hundreds). The calculations were performed in the temperature range of 0-1000K and compared to experimental values, showing a good quantitative and qualitative agreement. The various thermal contributions to the values of the elastic constants were studied as a function of temperature.

The results suggest that this method can be applied to calculate local elastic constants of real crystalline materials for local regions embedded within large crystalline structure. In addition, it can improve the calibration process of inter-atomic potentials, which typically employ the explicit deformation method [8, 10–16], that requires the generation of a consistent set of simulations under varying deformations, in order to obtain the elasticity tensor. The use of a single simulation, other than being simpler, convenient and accurate, has a lower risk for the spontaneous appearance of defects and other phases during direct force calculations.

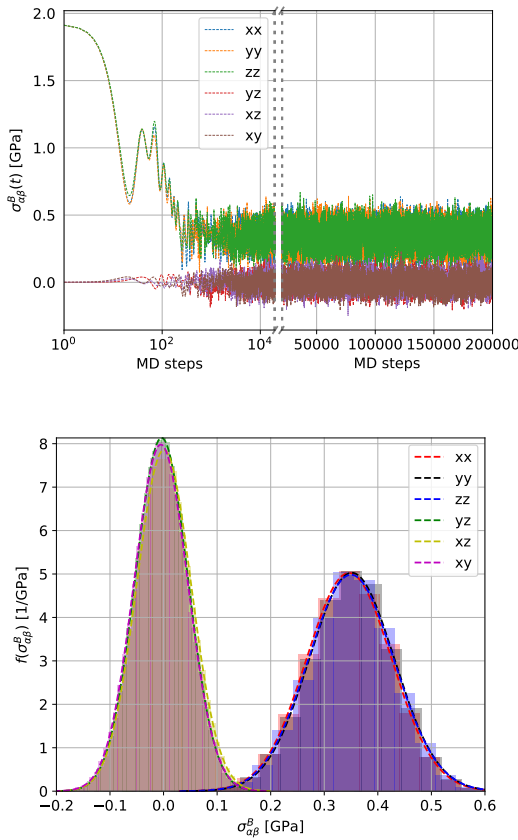


Figure 4. (Color online) Components of the instantaneous Born stress tensor (upper figure, eq. 25) for an NVT simulation of Copper at $T = 300\text{K}$ for which the volume is chosen such that the total pressure is zero (as obtained from Fig. 1). The lower figure shows the resulting histograms and fitted Gaussian distributions of the various Born stress tensor components.

-
- [1] Murray S Daw and Michael I Baskes. Embedded-atom method: Derivation and application to impurities, surfaces, and other defects in metals. *Physical Review B*, 29(12):6443, 1984.
 - [2] Ralph J Wolf, Khalid A Mansour, Myung W Lee, and John R Ray. Temperature dependence of elastic constants of embedded-atom models of palladium. *Physical Review B*, 46(13):8027, 1992.
 - [3] T Çağın, G Dereli, M Uludoğan, and MEHMET Tomak. Thermal and mechanical properties of some fcc transition metals. *Physical review B*, 59(5):3468, 1999.
 - [4] Somchart Chantasiriwan and Frederick Milstein. Higher-order elasticity of cubic metals in the embedded-atom method. *Physical Review B*, 53(21):14080, 1996.
 - [5] John R Ray, Michael C Moody, and Aneesur Rahman. Molecular dynamics calculation of elastic constants for a crystalline system in equilibrium. *Physical Review B*, 32(2):733, 1985.
 - [6] DR Squire, AC Holt, and WG Hoover. Isothermal elastic constants for argon. theory and monte carlo calculations. *Physica*, 42(3):388–397, 1969.
 - [7] JF Lutsko. Generalized expressions for the calculation of elastic constants by computer simulation. *Journal of applied physics*, 65(8):2991–2997, 1989.
 - [8] Germain Clavier, Nicolas Desbiens, Emeric Bourasseau, Véronique Lachet, Nadège Brusselle-Dupend, and Bernard Rousseau. Computation of elastic constants of solids using molecular simulation: comparison of constant volume and constant pressure ensemble methods. *Molecular Simulation*, 43(17):1413–1422, 2017.
 - [9] Dominik Lips and Philipp Maass. Stress-stress fluctuation formula for elastic constants in the npt ensemble. *Physical Review E*, 97(5):053002, 2018.
 - [10] Seyed Moein Rassoulinejad-Mousavi, Yijin Mao, and Yuwen Zhang. Evaluation of copper, aluminum, and nickel interatomic potentials on predicting the elastic properties. *Journal of Applied Physics*, 119(24):244304, 2016.
 - [11] Michael Griebel and Jan Hamaekers. Molecular dynamics simulations of the elastic moduli of polymer-carbon

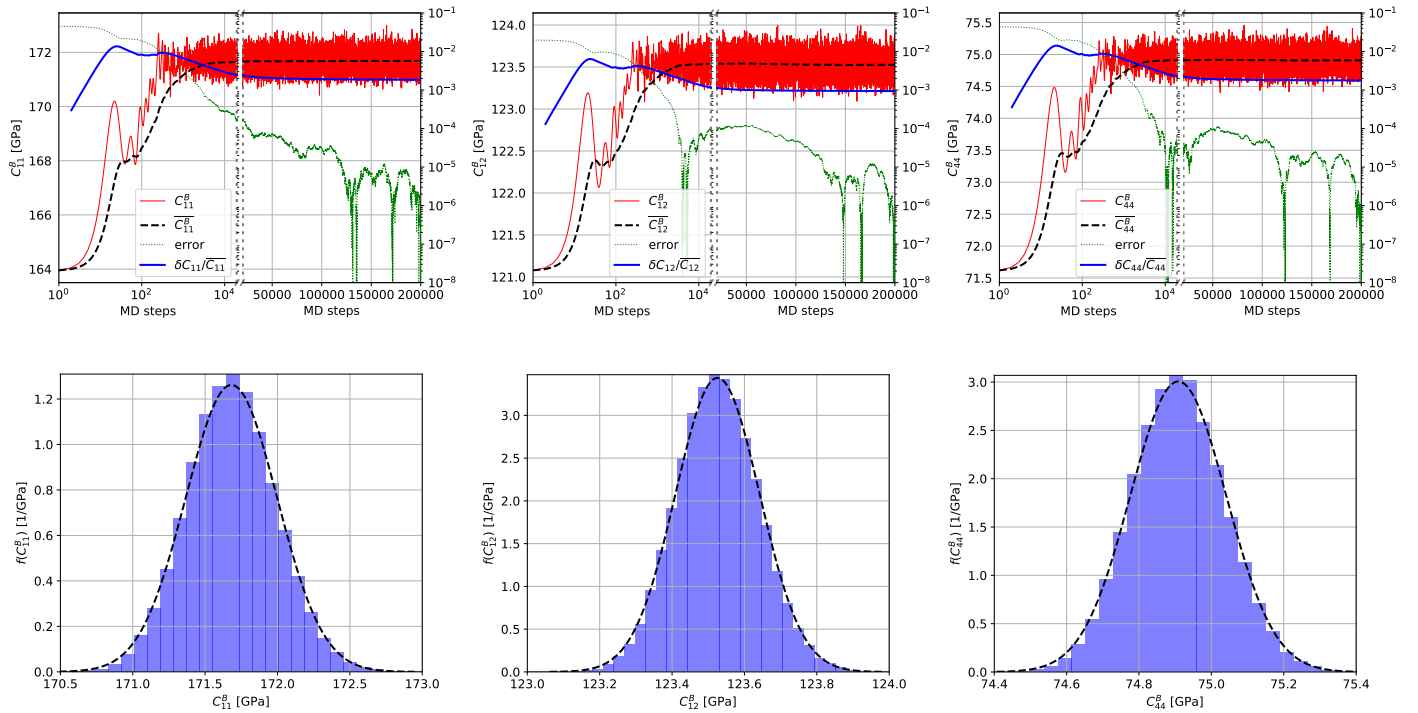


Figure 5. (Color online) Upper figures - the Born elastic constants (eq. 26): C_{11}^B (left upper figure), C_{12}^B (middle upper figure) and C_{44}^B (right upper figure), for an NVT simulation of Copper at $T = 300\text{K}$ (as described in Fig. 4). The instantaneous value, cumulative average, convergence error and ratio of the standard deviation to the mean are shown, as is detailed in Fig. 2. The lower figures shows the resulting histograms and fitted Gaussian distributions.

- nanotube composites. *Computer methods in applied mechanics and engineering*, 193(17-20):1773–1788, 2004.
- [12] DJ Quesnel, DS Rimai, and LP DeMejo. Elastic compliances and stiffnesses of the fcc lennard-jones solid. *Physical Review B*, 48(10):6795, 1993.
- [13] Oleg L Manevitch and Gregory C Rutledge. Elastic properties of a single lamella of montmorillonite by molecular dynamics simulation. *The Journal of Physical Chemistry B*, 108(4):1428–1435, 2004.
- [14] Priya Vashishta, Rajiv K Kalia, Aiichiro Nakano, and José Pedro Rino. Interaction potential for silicon carbide: A molecular dynamics study of elastic constants and vibrational density of states for crystalline and amorphous silicon carbide. *Journal of applied physics*, 101(10):103515, 2007.
- [15] Qing-Xiang Pei, Yong-Wei Zhang, and Vivek B Shenoy. Mechanical properties of methyl functionalized graphene: a molecular dynamics study. *Nanotechnology*, 21(11):115709, 2010.
- [16] Saaketh Desai and Alejandro Strachan. Lammmps driver tool for potential calibration. 2019.
- [17] L Huang, Levente Vitos, SK Kwon, Börje Johansson, and Rajeev Ahuja. Thermoelastic properties of random alloys from first-principles theory. *Physical Review B*, 73(10):104203, 2006.
- [18] Philipp Keuter, Denis Music, Volker Schnabel, Michael Stuer, and Jochen M Schneider. From qualitative to quantitative description of the anomalous thermoelastic behavior of v, nb, ta, pd and pt. *Journal of Physics: Condensed Matter*, 31(22):225402, 2019.
- [19] M Parrinello and A Rahman. Strain fluctuations and elastic constants. *The Journal of Chemical Physics*, 76(5):2662–2666, 1982.
- [20] Andrei A Gusev, Marcel M Zehnder, and Ulrich W Suter. Fluctuation formula for elastic constants. *Physical Review B*, 54(1):1, 1996.
- [21] Wataru Shinoda, Motoyuki Shiga, and Masuhiro Mikami. Rapid estimation of elastic constants by molecular dynamics simulation under constant stress. *Physical Review B*, 69(13):134103, 2004.
- [22] Glenn J Martyna, Douglas J Tobias, and Michael L Klein. Constant pressure molecular dynamics algorithms. *The Journal of chemical physics*, 101(5):4177–4189, 1994.
- [23] Glenn J Martyna, Mark E Tuckerman, Douglas J Tobias, and Michael L Klein. Explicit reversible integrators for extended systems dynamics. *Molecular Physics*, 87(5):1117–1157, 1996.
- [24] Mark E Tuckerman, Yi Liu, Giovanni Ciccotti, and Glenn J Martyna. Non-hamiltonian molecular dynamics: Generalizing hamiltonian phase space principles to non-hamiltonian systems. *The Journal of Chemical Physics*, 115(4):1678–1702, 2001.
- [25] Mark E Tuckerman, José Alejandro, Roberto López-Rendón, Andrea L Jochim, and Glenn J Martyna. A liouville-operator derived measure-preserving integrator for molecular dynamics simulations in the isothermal-isobaric ensemble. *Journal of Physics A: Mathematical and General*, 39(19):5629, 2006.
- [26] Mark Tuckerman. *Statistical mechanics: theory and molecular simulation*. Oxford university press, 2010.
- [27] Michael P Allen and Dominic J Tildesley. *Computer simulation of liquids*. Oxford university press, 2017.

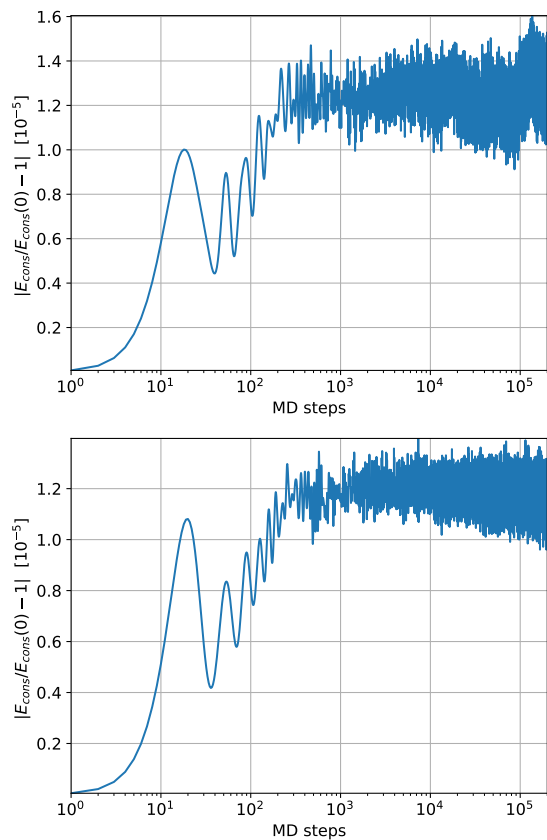


Figure 6. Relative error between the instantaneous conserved energy and the initial value, for NPT (upper figure, eq. B8) and NVT (upper figure, eq. C15) molecular dynamics simulations of Copper at $T = 300\text{K}$ and zero pressure (the simulations described in figures 2-3 and 4-5, respectively).

- [28] Glenn J Martyna, Michael L Klein, and Mark Tuckerman. Nosé–hoover chains: The canonical ensemble via continuous dynamics. *The Journal of chemical physics*, 97(4):2635–2643, 1992.
- [29] Shuichi Nosé. A unified formulation of the constant temperature molecular dynamics methods. *The Journal of chemical physics*, 81(1):511–519, 1984.
- [30] William G Hoover. Canonical dynamics: Equilibrium phase-space distributions. *Physical review A*, 31(3):1695, 1985.
- [31] Yu Mishin, MJ Mehl, DA Papaconstantopoulos, AF Voter, and JD Kress. Structural stability and lattice defects in copper: Ab initio, tight-binding, and embedded-atom calculations. *Physical Review B*, 63(22):224106, 2001.
- [32] RN Thurston. Wave propagation in fluids and normal solids. In *Physical acoustics*, pages 1–110. Elsevier, 1964.
- [33] Duane C Wallace. Thermoelasticity of stressed materials and comparison of various elastic constants. *Physical Review*, 162(3):776, 1967.
- [34] K Brugger. Thermodynamic definition of higher order elastic coefficients. *Physical Review*, 133(6A):A1611, 1964.
- [35] Duane C. Wallace. *Thermodynamics of crystals*. Wiley New York, 1972.
- [36] John R Ray and Aneesur Rahman. Statistical ensembles and molecular dynamics studies of anisotropic solids. *The Journal of chemical physics*, 80(9):4423–4428, 1984.
- [37] KW Wojciechowski. Constant thermodynamic tension monte carlo studies of elastic properties of a two-dimensional system of hard cyclic hexamers. *Molecular Physics*, 61(5):1247–1258, 1987.
- [38] John R Ray. Elastic constants and statistical ensembles in molecular dynamics. *Computer physics reports*, 8(3):109–151, 1988.
- [39] Kevin Van Workum, Kenji Yoshimoto, Juan J de Pablo, and Jack F Douglas. Isothermal stress and elasticity tensors for ions and point dipoles using ewald summations. *Physical Review E*, 71(6):061102, 2005.
- [40] J-L Barrat. Microscopic elasticity of complex systems. In *Computer Simulations in Condensed Matter Systems: From Materials to Chemical Biology Volume 2*, pages 287–307. Springer, 2006.
- [41] Max Born and Kun Huang. *Dynamical theory of crystal lattices*. Clarendon press, 1954.
- [42] WC Overton Jr and John Gaffney. Temperature variation of the elastic constants of cubic elements. i. copper. *Physical Review*, 98(4):969, 1955.
- [43] YA Chang and L Himmel. Temperature dependence of the elastic constants of cu, ag, and au above room temperature. *Journal of Applied Physics*, 37(9):3567–3572, 1966.
- [44] Haruo Yoshida. Construction of higher order symplectic integrators. *Physics letters A*, 150(5-7):262–268, 1990.
- [45] Masuo Suzuki. General theory of fractal path integrals with applications to many-body theories and statistical physics. *Journal of Mathematical Physics*, 32(2):400–407, 1991.
- [46] Y Wang, JJ Wang, H Zhang, VR Manga, SL Shang, LQ Chen, and ZK Liu. A first-principles approach to finite temperature elastic constants. *Journal of Physics: Condensed Matter*, 22(22):225404, 2010.
- [47] O Gülseren and RE Cohen. High-pressure thermoelasticity of body-centered-cubic tantalum. *Physical Review B*, 65(6):064103, 2002.
- [48] Hieu H Pham, Michael E Williams, Patrick Mahaffey, Miladin Radovic, Raymundo Arroyave, and Tahir Cagin. Finite-temperature elasticity of fcc al: Atomistic simulations and ultrasonic measurements. *Physical Review B*, 84(6):064101, 2011.
- [49] Steve Plimpton. Fast parallel algorithms for short-range molecular dynamics. *Journal of computational physics*, 117(1):1–19, 1995.

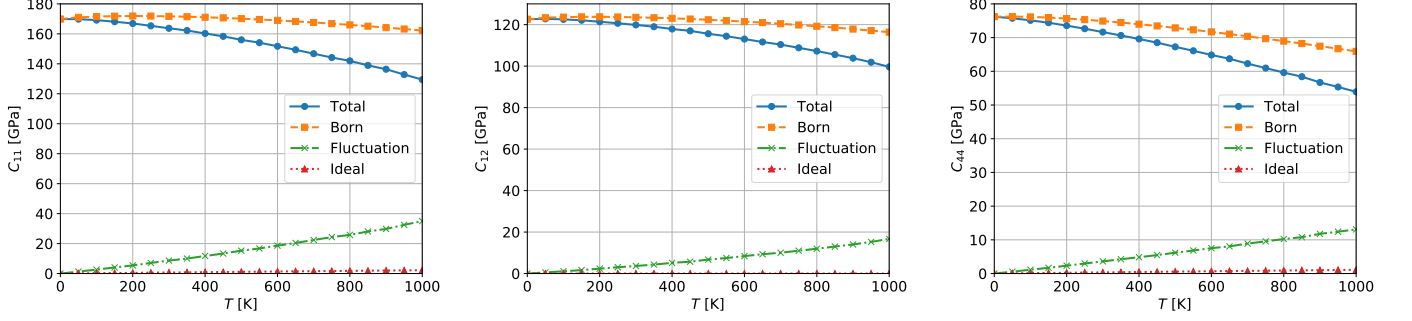


Figure 7. (Color online) The different terms contributing to the total isothermal elastic constants C_{11} (left pane), C_{12} (middle pane) and C_{44} (right pane) of Copper as a function of temperature (solid blue line) - the Born term (first term in eq. 21, dashed orange line), Born stress fluctuation term (minus the second term in eq. 21, dashed dotted green line) and the ideal gas kinetic term (minus the last term in eq. 21, dotted red line).

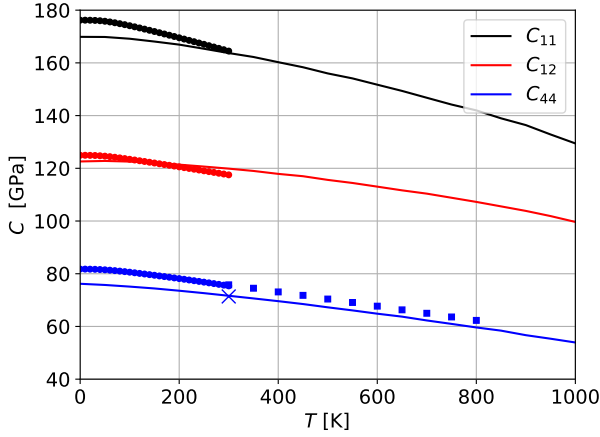


Figure 8. (Color online) The isothermal elastic constants C_{11} (black), C_{12} (red) and C_{44} (blue) of Copper as a function of temperature. Solid lines represent molecular dynamics calculations performed in this work (see text for details), circles represent experimental values in the temperature range 0-300K given in Ref. [42] and squares represent experimental values in the range 300-800K given in Ref. [43] for C_{44} . The blue X data point represents a calculated C_{44} result given in Ref. [10].

Appendix A: Elastic constants in the canonical ensemble

In the canonical ensemble, the free energy is given by:

$$\mathcal{F} = -k_B T \ln Z, \quad (\text{A1})$$

where the canonical partition function is given by:

$$\begin{aligned} Z &= \frac{1}{h^{3N}} \int d^3 \mathbf{p}^N \int_V d^3 \mathbf{r}^N e^{-\beta \mathcal{H}(\mathbf{r}^N, \mathbf{p}^N)} \\ &= \frac{1}{\prod_i^N \Lambda_i^3} \int_V d^3 \mathbf{r}^N e^{-\beta \mathcal{V}(\mathbf{r}^N)}, \end{aligned} \quad (\text{A2})$$

where $\beta = 1/k_B T$ and $\Lambda_i = \left(\frac{2\pi\hbar^2\beta}{m_i} \right)^{\frac{1}{2}}$ is the thermal de-Broglie wavelength. We note that in order calculate strain derivatives (i.e. as in equations 12-13), the $\frac{1}{\prod_i^N \Lambda_i^3}$ factor can be dropped, so that for the derivations presented in this appendix, we re-denote:

$$Z = \int_V d^3 \mathbf{r}^N e^{-\beta \mathcal{V}(\mathbf{r}^N)}. \quad (\text{A3})$$

Consider the canonical average of a configurational operator $A = A(\mathbf{r}^N)$:

$$\langle A \rangle = \frac{1}{Z} \int_V d^3 \mathbf{r}^N A(\mathbf{r}^N) e^{-\beta \mathcal{V}(\mathbf{r}^N)}. \quad (\text{A4})$$

In order to evaluate the strain derivative $\frac{\partial \langle A \rangle}{\partial \eta_{\alpha\beta}}$, we write the integral in terms of the reference configuration coordinates \mathbf{R} , since the strain derivative cannot be brought inside the integral, because the deformed volume V depends on η . Therefore, we write:

$$\int_V d^3 \mathbf{r}^N A(\mathbf{r}^N) e^{-\beta \mathcal{V}(\mathbf{r}^N)} = \int_{V_0} d^3 \mathbf{R}^N (\det \mathbf{J})^N A e^{-\beta \mathcal{V}}, \quad (\text{A5})$$

where the integrand in the RHS is understood to be evaluated at $\mathbf{r}(\mathbf{R})$. We can now write the strain derivative:

$$\begin{aligned} \frac{\partial}{\partial \eta_{\alpha\beta}} \int_V d^3 \mathbf{r}^N A(\mathbf{r}^N) e^{-\beta \mathcal{V}(\mathbf{r}^N)} &= \\ \int_{V_0} d^3 \mathbf{R}^N \frac{\partial}{\partial \eta_{\alpha\beta}} \left[(\det \mathbf{J})^N A e^{-\beta \mathcal{V}} \right], \end{aligned} \quad (\text{A6})$$

the integrand reads:

$$\begin{aligned} \frac{\partial}{\partial \eta_{\alpha\beta}} \left[(\det \mathbf{J})^N A e^{-\beta \mathcal{V}} \right] &= \\ e^{-\beta \mathcal{V}} (\det \mathbf{J})^N \left[A \frac{N}{\det(\mathbf{J})} \frac{\partial \det(\mathbf{J})}{\partial \eta_{\alpha\beta}} + \frac{\partial A}{\partial \eta_{\alpha\beta}} - \beta A \frac{\partial \mathcal{V}}{\partial \eta_{\alpha\beta}} \right]. \end{aligned}$$

Using the well known rule for the derivative of a determinant:

$$\frac{\partial \det(\mathbf{M})}{\partial M_{\alpha\beta}} = \det(\mathbf{M}) M_{\alpha\beta}^{-T}, \quad (\text{A7})$$

and eq. 3, it is readily shown that:

$$\frac{1}{\det(\mathbf{J})} \frac{\partial \det(\mathbf{J})}{\partial \eta_{\alpha\beta}} = \frac{1}{\det(\mathbf{J})} D_{\alpha\beta} \det(\mathbf{J}) = (2\boldsymbol{\eta} + \mathbf{I})_{\alpha\beta}^{-T}. \quad (\text{A8})$$

As a result, eq. A6 reads:

$$\begin{aligned} \frac{\partial}{\partial \eta_{\alpha\beta}} \left(\int_V d^3\mathbf{r}^N A(\mathbf{r}^N) e^{-\beta\mathcal{V}(\mathbf{r}^N)} \right) &= \\ \int_{V_0} d^3\mathbf{R}^N (\det \mathbf{J})^N \left[A(2\boldsymbol{\eta} + \mathbf{I})_{\alpha\beta}^{-T} + \frac{\partial A}{\partial \eta_{\alpha\beta}} - \beta A \frac{\partial \mathcal{V}}{\partial \eta_{\alpha\beta}} \right] e^{-\beta\mathcal{V}} &= \\ = \int_V d^3\mathbf{r}^N \left[A(2\boldsymbol{\eta} + \mathbf{I})_{\alpha\beta}^{-T} + \frac{\partial A}{\partial \eta_{\alpha\beta}} - \beta A \frac{\partial \mathcal{V}}{\partial \eta_{\alpha\beta}} \right] e^{-\beta\mathcal{V}}. & \end{aligned} \quad (\text{A9})$$

Using this for the particular case $A \equiv 1$, one finds:

$$\frac{1}{Z} \frac{\partial Z}{\partial \eta_{\alpha\beta}} = (2\boldsymbol{\eta} + \mathbf{I})_{\alpha\beta}^{-T} - \beta \left\langle \frac{\partial \mathcal{V}}{\partial \eta_{\alpha\beta}} \right\rangle. \quad (\text{A10})$$

Differentiation of eq. A4 using the derivative product rule and equations A9-A10, results in the general strain derivative rule:

$$\frac{\partial \langle A \rangle}{\partial \eta_{\alpha\beta}} = \left\langle \frac{\partial A}{\partial \eta_{\alpha\beta}} \right\rangle - \beta \left[\left\langle A \frac{\partial \mathcal{V}}{\partial \eta_{\alpha\beta}} \right\rangle - \langle A \rangle \left\langle \frac{\partial \mathcal{V}}{\partial \eta_{\alpha\beta}} \right\rangle \right]. \quad (\text{A11})$$

For an EAM potential of the form 15, we can write:

$$\begin{aligned} \frac{\partial \mathcal{V}}{\partial \eta_{\alpha\beta}} &= \sum_i \frac{\partial \mathcal{V}}{\partial \mathbf{r}_i} \cdot \frac{\partial \mathbf{r}_i}{\partial \eta_{\alpha\beta}} = - \sum_i F_{i,\gamma} \frac{\partial r_{i,\gamma}}{\partial \eta_{\alpha\beta}} \\ &= - \sum_i \sum_{j \neq i} F_{ij} \frac{r_{ij,\gamma}}{r_{ij}} \frac{\partial r_{i,\gamma}}{\partial \eta_{\alpha\beta}} \\ &= - \frac{1}{2} \sum_i \sum_{j \neq i} \left(F_{ij} \frac{r_{ij,\gamma}}{r_{ij}} \frac{\partial r_{i,\gamma}}{\partial \eta_{\alpha\beta}} + F_{ji} \frac{r_{ji,\gamma}}{r_{ji}} \frac{\partial r_{j,\gamma}}{\partial \eta_{\alpha\beta}} \right) \\ &= - \frac{1}{2} \sum_i \sum_{j \neq i} F_{ij} \frac{r_{ij,\gamma}}{r_{ij}} \frac{\partial r_{ij,\gamma}}{\partial \eta_{\alpha\beta}} = - \frac{1}{2} \sum_{i < j} \frac{F_{ij}}{r_{ij}} \frac{\partial r_{ij}^2}{\partial \eta_{\alpha\beta}}, \end{aligned}$$

where in the last term, the summation is over ordered pairs. From eq. 4 it is evident that:

$$\frac{\partial r^2}{\partial \eta_{\alpha\beta}} = 2R_\alpha R_\beta, \quad (\text{A12})$$

and, more generally, for any radial function $f = f(r)$, we have:

$$D_{\alpha\beta} f = \frac{\partial f}{\partial \eta_{\alpha\beta}} = \frac{\partial f}{\partial \eta_{\beta\alpha}} = \frac{df}{dr} \frac{R_\alpha R_\beta}{r}. \quad (\text{A13})$$

Hence, we can finally write:

$$\frac{\partial \mathcal{V}}{\partial \eta_{\alpha\beta}} = \frac{\partial \mathcal{V}}{\partial \eta_{\beta\alpha}} = D_{\alpha\beta} \mathcal{V} = - \sum_{i < j} F_{ij} \frac{R_{ij,\alpha} R_{ij,\beta}}{r_{ij}}. \quad (\text{A14})$$

From eq. A10 it follows that:

$$\frac{\partial \mathcal{F}}{\partial \eta_{\alpha\beta}} = \left\langle \frac{\partial \mathcal{V}}{\partial \eta_{\alpha\beta}} \right\rangle - k_B T N (2\boldsymbol{\eta} + \mathbf{I})_{\alpha\beta}^{-T}, \quad (\text{A15})$$

which is a symmetric tensor. Hence, eq. A15, when evaluated at zero strain, proves equations 23 and 25.

Next, in order to evaluate the isothermal elastic constant defined by eq. 13, consider the second derivative tensor:

$$D_{\alpha\beta} D_{\gamma\delta} \mathcal{F} = D_{\alpha\beta} \left[\left\langle \frac{\partial \mathcal{V}}{\partial \eta_{\gamma\delta}} \right\rangle - k_B T N (2\boldsymbol{\eta} + \mathbf{I})_{\gamma\delta}^{-T} \right]. \quad (\text{A16})$$

In order to evaluate the second term, we use the following identity for the derivative of a matrix inverse:

$$\frac{\partial M_{\delta\gamma}^{-1}}{\partial M_{\alpha\beta}} = -M_{\delta\alpha}^{-1} M_{\beta\gamma}^{-1}, \quad (\text{A17})$$

which results in the relation:

$$\begin{aligned} D_{\alpha\beta} \left[(2\boldsymbol{\eta} + \mathbf{I})_{\gamma\delta}^{-T} \right] &= - (2\boldsymbol{\eta} + \mathbf{I})_{\delta\alpha}^{-1} (2\boldsymbol{\eta} + \mathbf{I})_{\beta\gamma}^{-1} \\ &\quad - (2\boldsymbol{\eta} + \mathbf{I})_{\delta\beta}^{-1} (2\boldsymbol{\eta} + \mathbf{I})_{\alpha\gamma}^{-1}. \end{aligned} \quad (\text{A18})$$

In order to evaluate the first term in A16, we use the identity A11:

$$\begin{aligned} \frac{\partial}{\partial \eta_{\alpha\beta}} \left\langle \frac{\partial \mathcal{V}}{\partial \eta_{\gamma\delta}} \right\rangle &= \\ \left\langle \frac{\partial^2 \mathcal{V}}{\partial \eta_{\alpha\beta} \partial \eta_{\gamma\delta}} \right\rangle - \beta \left[\left\langle \frac{\partial \mathcal{V}}{\partial \eta_{\gamma\delta}} \frac{\partial \mathcal{V}}{\partial \eta_{\alpha\beta}} \right\rangle - \left\langle \frac{\partial \mathcal{V}}{\partial \eta_{\gamma\delta}} \right\rangle \left\langle \frac{\partial \mathcal{V}}{\partial \eta_{\alpha\beta}} \right\rangle \right] &= \\ = \left\langle \frac{\partial^2 \mathcal{V}}{\partial \eta_{\alpha\beta} \partial \eta_{\gamma\delta}} \right\rangle - \frac{V^2}{k_B T} [\langle \sigma_{\alpha\beta}^B \sigma_{\gamma\delta}^B \rangle - \langle \sigma_{\alpha\beta}^B \rangle \langle \sigma_{\gamma\delta}^B \rangle]. & \end{aligned} \quad (\text{A19})$$

We note that the second term is a symmetric tensor with respect to $\alpha \leftrightarrow \beta$ and $\gamma \leftrightarrow \delta$. In order to evaluate the first term, we differentiate eq. A14:

$$\begin{aligned} \frac{\partial^2 \mathcal{V}}{\partial \eta_{\alpha\beta} \partial \eta_{\gamma\delta}} &= \frac{\partial}{\partial \eta_{\alpha\beta}} \left(- \sum_{i < j} F_{ij} \frac{R_{ij,\gamma} R_{ij,\delta}}{r_{ij}} \right) \\ &= - \sum_{i < j} \left[\frac{R_{ij,\gamma} R_{ij,\delta}}{r_{ij}} \frac{\partial F_{ij}}{\partial \eta_{\alpha\beta}} + R_{ij,\gamma} R_{ij,\delta} F_{ij} \frac{\partial}{\partial \eta_{\alpha\beta}} \left(\frac{1}{r_{ij}} \right) \right]. \end{aligned} \quad (\text{A20})$$

Using the identity A13, we get:

$$\frac{\partial}{\partial \eta_{\alpha\beta}} \left(\frac{1}{r} \right) = -\frac{R_{\alpha} R_{\beta}}{r^3}, \quad (\text{A21})$$

and using eq. 17 and the identity A13 gives:

$$\begin{aligned} \frac{\partial F_{ij}}{\partial \eta_{\alpha\beta}} &= (v''(r_{ij}) + [F'(\rho_i) + F'(\rho_j)] \rho''(r_{ij})) \frac{R_{ij,\alpha} R_{ij,\beta}}{r_{ij}} \\ &+ \rho'(r_{ij}) \frac{\partial}{\partial \eta_{\alpha\beta}} [F'(\rho_i) + F'(\rho_j)]. \end{aligned} \quad (\text{A22})$$

In order to evaluate the last term in eq. A22, we write:

$$\begin{aligned} \frac{\partial}{\partial \eta_{\alpha\beta}} F'(\rho_i) &= F''(\rho_i) \frac{\partial \rho_i}{\partial \eta_{\alpha\beta}} = F''(\rho_i) \sum_{k \neq i} \frac{\partial \rho}{\partial \eta_{\alpha\beta}} \Big|_{r_{ik}} \\ &= F''(\rho_i) \sum_{k \neq i} \rho'(r_{ik}) \frac{R_{ik,\alpha} R_{ik,\beta}}{r_{ik}^2}, \end{aligned} \quad (\text{A23})$$

where in the last step the identity A13 was used again. Plugging equations A21-A22 back in eq. A20 gives:

$$\begin{aligned} \frac{\partial^2 \mathcal{V}}{\partial \eta_{\alpha\beta} \partial \eta_{\gamma\delta}} &= D_{\alpha\beta} D_{\gamma\delta} \mathcal{V} = \sum_{i < j} X_{ij} \frac{R_{ij,\alpha} R_{ij,\beta} R_{ij,\gamma} R_{ij,\delta}}{r_{ij}^2} \\ &+ \sum_i \left(\sum_{k \neq i} \frac{R_{ik,\alpha} R_{ik,\beta}}{r_{ik}^2} \rho'(r_{ik}) \right) \left(\sum_{k \neq i} \frac{R_{ik,\gamma} R_{ik,\delta}}{r_{ik}^2} \rho'(r_{ik}) \right), \end{aligned} \quad (\text{A24})$$

where X_{ij} is defined by eq. 27, and we have used the fact that the resulting expression defines a symmetric tensor with respect to $\alpha \leftrightarrow \beta$ and $\gamma \leftrightarrow \delta$.

Finally, when evaluated at zero strain ($\boldsymbol{\eta} = \mathbf{0}$, $\mathbf{R} = \mathbf{r}$), the combination of equations A16, A18, A19 and A24 proves the relations 21 and 26-28.

Appendix B: Equations of motion in the NVT ensemble

In this appendix we list the equations of motion of the widely used Nose-Hoover-Chains method [26–28], which was used in the calculations performed in this work. We use a chain of M thermostats with coordinates η_j and momenta p_{η_j} . The equations of motions for the $i = 1 \dots N$ particles are:

$$\frac{d\mathbf{r}_i}{dt} = \frac{\mathbf{p}_i}{m_i}, \quad (\text{B1})$$

$$\frac{d\mathbf{p}_i}{dt} = \mathbf{F}_i - \left(\frac{p_{\eta_1}}{Q_1} \right) \mathbf{p}_i. \quad (\text{B2})$$

The equations of motion for the $j = 1 \dots M$ thermostat variables are given by:

$$\frac{d\eta_j}{dt} = \frac{p_{\eta_j}}{Q_j}, \quad (\text{B3})$$

$$\frac{dp_{\eta_j}}{dt} = \begin{cases} G_j - \left(\frac{p_{\eta_{j+1}}}{Q_{j+1}} \right) p_{\eta_j}, & j = 1 \dots M-1 \\ G_M, & j = M \end{cases} \quad (\text{B4})$$

where the forces are:

$$G_j = \begin{cases} \sum_i \frac{p_i^2}{m_i} - g k_B T, & j = 1 \\ \frac{p_{\eta_{j-1}}^2}{Q_{j-1}} - k_B T, & j = 2 \dots M \end{cases} \quad (\text{B5})$$

with the number of degrees of freedom:

$$g = 3(N-1). \quad (\text{B6})$$

The thermostat “masses” Q_j can be written in terms of a thermostat relaxation timescale τ_T [28]:

$$Q_j = \begin{cases} g k_B T \tau_T^2, & j = 1 \\ k_B T \tau_T^2, & j = 2 \dots M \end{cases} \quad (\text{B7})$$

The non-Hamiltonian system B1-B4 has the conserved quantity [26, 28]:

$$E_{\text{cons}} = \mathcal{H} + \sum_{j=1}^M \frac{p_{\eta_j}^2}{2Q_j} + g k_B T \eta_1 + \sum_{j=2}^M k_B T \eta_j, \quad (\text{B8})$$

where \mathcal{H} is the true Hamiltonian given by eq. 14.

Appendix C: Equations of motion in the NPT ensemble

In this appendix we list the equations of motion in the widely used Nose-Hoover-Chains method in the isothermal-isobaric (NPT) ensemble [22, 25–27], which was used in the calculations performed in this work. As in appendix B, we use a chain of M thermostats whose coordinates and momenta are η_j and p_{η_j} , which are coupled the the equations of motion of the N particles. In the NPT ensemble, the volume $V = V(t)$ is treated as a dynamical variable via the generalized coordinate:

$$\epsilon(t) = \frac{1}{3} \ln \left(\frac{V(t)}{V(0)} \right), \quad (\text{C1})$$

whose momentum p_{ϵ} is coupled to an additional chain of M' thermostats with coordinates η'_j and momenta p'_{η_j} . The equations of motions for the $i = 1 \dots N$ particles are:

$$\frac{d\mathbf{r}_i}{dt} = \frac{\mathbf{p}_i}{m_i} + \frac{p_{\epsilon}}{W} \mathbf{r}_i, \quad (\text{C2})$$

$$\frac{d\mathbf{p}_i}{dt} = \mathbf{F}_i - \left(1 + \frac{3}{g} \right) \left(\frac{p_{\epsilon}}{W} \right) \mathbf{p}_i - \left(\frac{p_{\eta_1}}{Q_1} \right) \mathbf{p}_i, \quad (\text{C3})$$

The equations of motion for the barostat variables are:

$$\frac{d\epsilon}{dt} = \frac{p_\epsilon}{W}, \quad (C4)$$

$$\frac{d\eta'_j}{dt} = \frac{p_{\eta'_j}}{Q'_j}, \quad (C10)$$

$$\frac{dp_\epsilon}{dt} = 3(P_{inst}V - PV) + \frac{3}{g} \sum_{i=1}^N \frac{p_i^2}{m_i} - \left(\frac{p_{\eta'_1}}{Q'_1} \right) p_\epsilon, \quad (C5)$$

$$\frac{dp_{\eta'_j}}{dt} = \begin{cases} G'_j - \left(\frac{p_{\eta'_{j+1}}}{Q'_{j+1}} \right) p_{\eta'_j}, & j = 1 \dots M' - 1 \\ G'_{M'}, & j = M' \end{cases} \quad (C11)$$

where P is the applied external pressure and the instantaneous pressure is given by the virial theorem:

$$P_{inst}V = \frac{1}{3} \sum_i \frac{p_i^2}{m_i} + \frac{1}{3} \sum_{i < j} F_{ij} r_{ij}. \quad (C6)$$

The equations of motion for the $j = 1 \dots M$ particle-coupled thermostat variables are given by:

$$\frac{d\eta_j}{dt} = \frac{p_{\eta_j}}{Q_j}, \quad (C7)$$

$$\frac{dp_{\eta_j}}{dt} = \begin{cases} G_j - \left(\frac{p_{\eta_{j+1}}}{Q_{j+1}} \right) p_{\eta_j}, & j = 1 \dots M - 1 \\ G_M, & j = M \end{cases} \quad (C8)$$

where the forces are:

$$G_j = \begin{cases} \sum_i \frac{p_i^2}{m_i} - g k_B T, & j = 1 \\ \frac{p_{\eta_{j-1}}^2}{Q_{j-1}} - k_B T, & j = 2 \dots M \end{cases} \quad (C9)$$

The equations of motion for the $j = 1 \dots M'$ barostat-coupled thermostat variables are given by:

where the forces are:

$$G'_j = \begin{cases} \frac{p_\epsilon^2}{W} - k_B T, & j = 1 \\ \frac{p_{\eta'_{j-1}}^2}{Q'_{j-1}} - k_B T, & j = 2 \dots M' \end{cases} \quad (C12)$$

The particle-coupled thermostat masses Q_j are given in terms of a thermostat relaxation timescale τ_T as in B7, while the barostat mass W and the barostat-coupled thermostat masses Q'_j are written in terms of a barostat relaxation timescale τ_p as [23, 28]:

$$W = g k_B T \tau_p^2, \quad (C13)$$

$$Q'_j = k_B T \tau_p^2. \quad (C14)$$

The non-Hamiltonian system C2-C11 has the conserved quantity [22, 25, 26]:

$$E_{\text{cons}} = \mathcal{H} + PV + \frac{p_\epsilon^2}{2W} + \sum_{j=1}^M \frac{p_{\eta_j}^2}{2Q_j} + \sum_{j=1}^{M'} \frac{p_{\eta'_j}^2}{2Q'_j} + g k_B T \eta_1 + \sum_{j=2}^M k_B T \eta_j + \sum_{j=1}^{M'} k_B T \eta'_j. \quad (C15)$$